

Theoretical comparison of the energy harvesting capability among various electrostatic mechanisms from structure aspect

Chengkuo Lee^{a,b,*}, Ye Mei Lim^a, Bin Yang^b, Rama Krishna Kotlanka^b, Chun-Huat Heng^a, Johnny Han He^b, Min Tang^b, Jin Xie^b, Hanhua Feng^b

^a Department of Electrical & Computer Engineering, National University of Singapore, 4 Engineering Drive 3, Singapore 117576, Republic of Singapore

^b Institute of Microelectronics, Agency for Science, Technology and Research (A*STAR), 11 Science Park Road, Singapore 117685, Republic of Singapore

ARTICLE INFO

Article history:

Received 1 October 2008

Received in revised form 2 February 2009

Accepted 6 February 2009

Available online 28 February 2009

Keywords:

Power MEMS

Energy scavenger

Energy harvester

Electrostatic

Capacitive

Vibration

ABSTRACT

This paper provides (i) a comparison of the energy harvesting capabilities of three different electrostatic mechanisms, and (ii) discussion on the relations among the contributing parameters involved in maximizing the energy output that can be harvested from an electrostatic microelectromechanical system (MEMS) device. The three mechanisms considered in this paper are namely the in-plane overlap, in-plane gap closing and out-of-plane gap closing converters. In this analytical modeling, the mass of the movable loads as well as the cross-sectional areas of the devices' active regions were set to be the same for all the mechanisms, while we assumed these electrostatic mechanisms are operated in ideal vacuum environment. A maximum output energy density of $0.547 \mu\text{J mm}^{-3}$ has been obtained for the case in which the movable load has a volume of 5 mm^3 .

© 2009 Published by Elsevier B.V.

1. Introduction

Traditionally, electronic devices have relied on batteries for power as they are reliable, easily accessible and convenient to use. However, batteries can only provide energy over a finite period of time, after which they will have to be changed. Since batteries have to be replaced periodically, their usage is limited to applications in which battery replacement is convenient. This suggests that for autonomously operating remote devices where battery replacement is difficult, batteries are not a perfect solution in the long run. In view of this, researchers have been motivated to harvest energy from the environment to power such remote sensors, with ambient vibrations being one such source of energy. By combining energy harvester with rechargeable battery, we can create battery-based power source of infinite lifetime ideally. At this moment, energy harvested from ambient vibrations typically produces power in the microwatt range [1], and this makes them suitable candidates to power microelectromechanical system (MEMS) sensors in remote applications as these devices have power requirements of the same

order of magnitude [2]. A wide range of vibration-powered MEMS energy harvesters have been proposed or demonstrated so far [1–3]. The most investigated MEMS energy harvesters are using piezoelectric, electromagnetic and electrostatic schemes.

Piezoelectric vibration energy harvesters typically consist of a bulk mass assembled or integrated to a cantilever, doubly clamped beam or membrane comprising a piezoelectric capacitor. These devices are based on a resonance principle and they give maximum power output under their resonance conditions, for which the deflection amplitude is maximized. For example, Fang et al. has reported a cantilever-based piezoelectric transducer that provides $2.16 \mu\text{W}$ regarding to ambient vibration at 609 Hz [4]. Multiple piezoelectric bimorph cantilevers have been assembled together for powering autonomous sensors from background vibrations with a wide range of frequency [5]. Lefeuvre et al. have reported a comparison among four vibration-powered piezoelectric energy harvesters [6].

In fact, the first concept of a vibration based energy harvester was presented by Williams and Yates in 1995, and was an electromagnetic based approach [7]. Shearwood and Yates report the first measured results electromagnetic MEMS energy harvester [8]. The device contains a planar coil on the backside of a substrate with a cavity on the top, a magnet of mass 2.4 mg on a flexible membrane above the cavity. The average output power has been reported as $0.33 \mu\text{W}$ versus 4.4 kHz vibration. Several review articles provides the insight on various electromagnetic mechanisms [9,10].

* Corresponding author at: Department of Electrical & Computer Engineering, National University of Singapore, 4 Engineering Drive 3, Singapore 117576, Republic of Singapore. Tel.: +65 6516 5865; fax: +65 6779 1103.

E-mail addresses: vincentleenus@yahoo.com.sg, elelc@nus.edu.sg, leeck@ime.a-star.edu.sg (C. Lee).

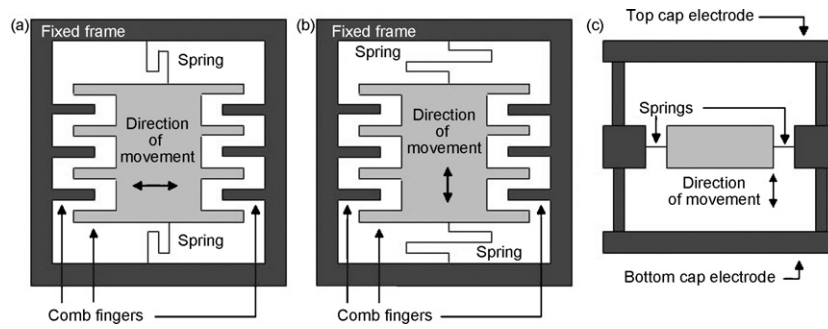


Fig. 1. The three different electrostatic mechanisms. The dark areas represent the fixed elements and the light areas, the movable elements. (a) In-plane overlap converter. (b) In-plane gap-closing converter. (c) Out-of-plane gap closing converter.

The first electrostatic comb based energy harvester has been reported by Chandrakasan's group at MIT in 2001 [11]. In this paper, authors also investigated the energy conversion cycle in terms of constant charge and constant voltage schemes. Additionally, Roundy et al. have developed a mathematic model for optimizing the output power for three different kinds of electrostatic mechanisms, namely, in-plane overlap, in-plane gap closing, and out-of-plane gap closing. With consideration of air damping effect, it is concluded that the out-of-plane gap closing mechanism face significant air damping [2,3]. A non-resonant based electrostatic MEMS of out-of-plane gap closing mechanism has been proposed by Miao et al. [12]. Output voltages of up to 220 V were obtained in which it is referring to a net generated power of 120 nJ per cycle. On the other hand, Kuehne et al., has reported a resonant based electrostatic MEMS of out-of-plane gap closing mechanism in 2008 [13]. This device provides an output power of 4.28 μW under vibration with frequency of 1 kHz and amplitude of 1.96 m/s^2 , i.e., 0.2 g. More recently, Chiu et al. have developed an electrostatic MEMS energy harvester of in-plane gap closing mechanism with a 1 cm^2 chip area. AC output power of 1.2 μW with a load of 5 $\text{M}\Omega$ was measured at 1.87 kHz [14,15]. Mitcheson et al., have surveyed and tabulated key features of published energy harvesters [16]. Generally speaking, it was found that the electrostatic mechanism has the lowest energy harvesting capabilities amongst all the three energy harvesters [16]. Despite having the lowest energy harvesting capability, electrostatic energy harvesters do have specific advantages and areas of application. The electrostatic devices are mainly made of silicon by using semiconductor fabrication technology such that it facilitates CMOS integration. In other words, electrostatic energy harvesters could be a way for realizing self-powered integrated circuits as an on-chip power source. However, due to the air damping effect, the two plates of electrodes can not come to contact so as to achieve the maximum capacitance state in the electrostatic energy harvesters. It is the main reason which leads to low energy harvesting capability of electrostatic approach.

On the other hand, wafer level vacuum packaging technologies have been demonstrated by several groups [17]. The reported technologies include: wafer bonding based on anodic bonding technique [17,18] and metal solder as bonding interface [19,20], and wafer level encapsulation based on poly-Si layer [21] and metal layer [22]. These papers point out that we can create a wafer level vacuum packaging for electrostatic MEMS energy harvesters such that the air damping effect can be significantly removed. Thereafter we can expect to have the maximum capacitance (C_{max}) to be achieved when two electrodes contact each other with dielectric isolation layer as a spacer. Although a few electrostatic MEMS energy harvesters have been reported, we lack of design trade-off in the case of vacuum operation. The intention of this paper is to study its intrinsic energy output and to study how device configurations can affect energy output. The comparison is made for three major electrostatic mechanisms (i.e., in-plane overlap, in-plane gap clos-

ing, and out-of-plane gap closing mechanisms) in terms of output energy density which is obtained by normalizing the output energy with the device volume.

2. Theoretical background

As illustrated in Fig. 1, all of these operate via a variable capacitance that can oscillate between a maximum and minimum value. However, what distinguishes the different mechanisms from each other is the manner in which this varying capacitance is achieved. The in-plane overlap converter varies its capacitance by changing the overlap area between electrode fingers, the in-plane gap closing converter varies its capacitance by changing the gap between electrode fingers and the out-of-plane gap closing converter varies its capacitance by changing the gap between two large electrode plates [2]. Typically, there are two methods in which the energy conversion can take place, and they are namely the voltage-constrained conversion method and the charge-constrained conversion method. Regardless of the harvesting mechanism used, the basic principle behind the energy conversion process in electrostatic scheme is the same. The charge-constrained method is more popular over the voltage-constrained method as it requires just one external charge reservoir instead of two [2,11]. For this reason, the discussion will just be focused on the charge-constrained method. For the purposes of describing how the energy harvesting process works, a movable mass as an electrode of variable capacitor will be assumed in the explanation of the charge-constrained energy conversion cycle.

When the structure is vibrated, the energy conversion cycle starts when the capacitance of the structure momentarily reaches an effective maximum value of C_{max} . This charging process is represented by the path from point A to point B in Fig. 2. At the point B, an external charge reservoir deposits a charge across the electrodes. As a result, an effective potential difference of V_{start} can be measured across the electrodes. The energy that is stored in the system after charging can be expressed as

$$E_B = \frac{1}{2} C_{\text{max}} V_{\text{start}}^2 \quad (1)$$

After the variable capacitor has been charged to V_{start} , the electrodes are electrically isolated and the physical separation between the electrode plates is forced to increase due to inertial motion of movable electrode. It is being represented in Fig. 2 as the path from point B to point C. This is the actual step in which mechanical energy is being converted to electrical energy. With an aid of a switch in the energy harvesting circuits [2], the electrodes are electrically isolated such that the charges on the electrodes are forced to remain constant from point B to point C. At the same time, the increase in physical separation causes the capacitance of the capacitor to decrease to a minimum value of C_{min} . These two factors lead to an increase in the potential difference across the capacitor.

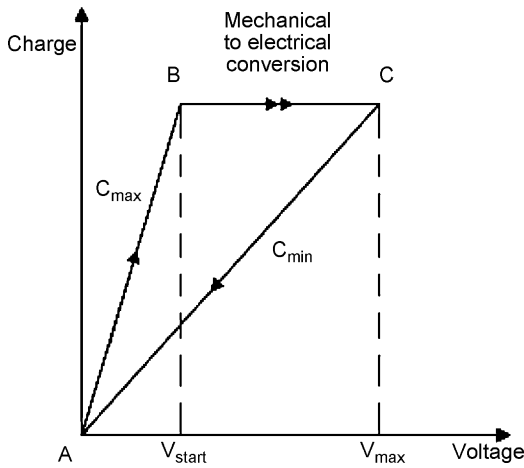


Fig. 2. The charge-constrained energy conversion cycle.

Specifically, the potential difference increases from V_{start} to V_{max} . When the capacitance has reached C_{min} , the electrical energy stored in the system can be expressed by

$$E_C = \frac{1}{2} C_{min} V_{max}^2 \quad (2)$$

The last step involved in the energy conversion cycle is the discharging of the charge on the variable capacitor back into the charge reservoir. This is represented by the path from point C to point A in Fig. 2, and it concludes one energy conversion cycle. Hence, the

amount of energy converted from mechanical to electrical energy in one conversion cycle is

$$E_{conv} = E_C - E_B = \frac{1}{2} (C_{min} V_{max}^2 - C_{max} V_{start}^2) \quad (3)$$

By taking into account charge conservation, there is the following relation that we observe the same charges from point B to point C

$$C_{max} V_{start} = C_{min} V_{max} \quad (4)$$

The energy being converted in one energy cycle can thus be rewritten as

$$E_{conv} = \frac{1}{2} V_{start}^2 \frac{C_{max}}{C_{min}} (C_{max} - C_{min}) \quad (5)$$

$$= \frac{1}{2} V_{start} V_{max} (C_{max} - C_{min}) \quad (6)$$

As suggested by Refs. [2] and [11], a parallel capacitor, C_{par} , will be connected in parallel to the MEMS capacitor to limit the maximum voltage that is reached by the system. This is required in practice because circuits are only able to tolerate voltages below a certain limit, above which the switches in the circuit will break down. With the addition of such a parallel capacitor, the following equations will be of use in the analysis

$$V_{max} = \frac{C_{max} + C_{par}}{C_{min} + C_{par}} V_{start} \quad (7)$$

$$E_{conv} = \frac{1}{2} V_{start}^2 \frac{C_{max} + C_{par}}{C_{min} + C_{par}} (C_{max} - C_{min}) \quad (8)$$

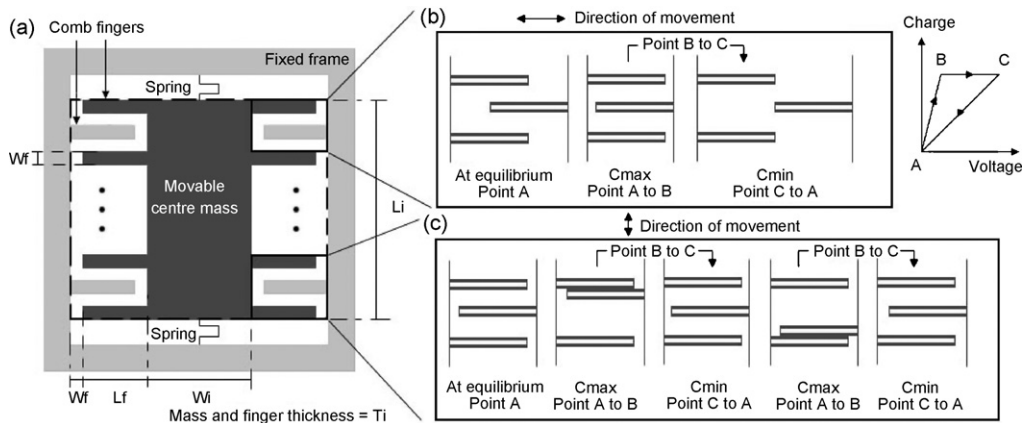


Fig. 3. In-plane movement mechanism. (a) Top view of the in-plane overlap and in-plane gap closing structure. The dotted region is the active volume of the device. (b) One mechanical oscillation cycle for one comb set in the in-plane overlap converter. (c) One mechanical oscillation cycle for one comb set in the in-plane gap closing converter.

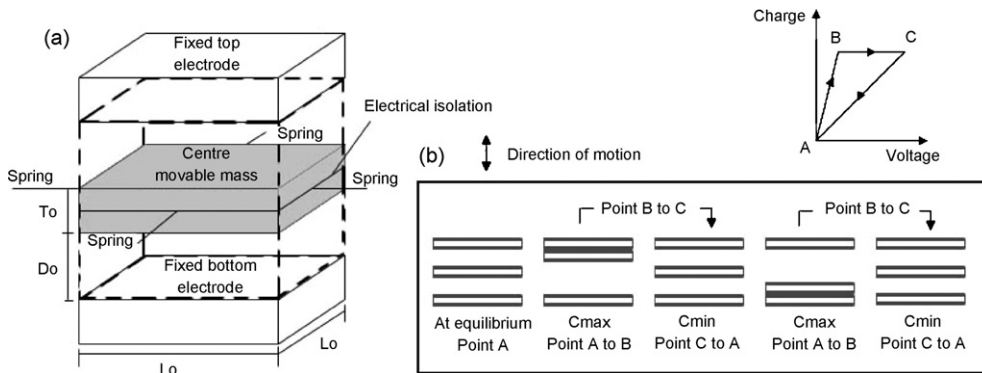


Fig. 4. Out-of-plane movement mechanism. (a) Side view of the out-of-plane gap closing structure. The dotted region is the active volume of the device. (b) One mechanical oscillation cycle for the out-of-plane gap closing converter. For the centre movable mass, there is an electrical isolation in the middle which allows for two energy conversion cycles in one mechanical oscillation.

$$= \frac{1}{2} V_{\text{start}} V_{\text{max}} (C_{\text{max}} - C_{\text{min}}) \quad (9)$$

3. Device structure and operation

The energy harvesting capabilities between the in-plane overlap, in-plane gap closing and out-of-plane gap closing converters will be compared to determine which one of these mechanisms can produce the highest amount of energy output per unit volume. For this comparison, specific design topologies were developed for each of these cases, and they are illustrated in Fig. 3(a) and Fig. 4(a). The main reason for choosing these designs is that they are relatively intuitive and straightforward.

Each of these structures consists of movable as well as fixed components, and they have been labeled respectively in Figs. 3 and 4(a). In addition, the regions which have been highlighted with dotted lines (in Figs. 3 and 4(a)) are the active volumes that the output power will be normalized against later. These volumes are chosen because it is mainly within these defined active regions that the energy conversion is taking place. In addition, all of these structures are assumed to have a 0.1 μm silicon nitride (Si_3N_4) dielectric coating. One of the purposes of this coating is to electrically isolate the electrodes to ensure that there is no charge exchange even if the plates were to come in contact with each other. On top of that, this dielectric coating also serves the purpose of allowing the minimum distance between electrodes to be minimized. In fact, with this coating, the plates can even come into contact with each other during vibration cycle when we assume the energy harvester is packaged in ideal vacuum environment. This allows the maximum achievable C_{max} to become greater and this increases the energy output. For both the in-plane overlap and in-plane gap closing mechanisms, the comb fingers are the electrodes that are responsible for the energy conversion. Fig. 3(b) and (c) illustrate the physical movement of one set of combs during one mechanical oscillation for the in-plane overlap and in-plane gap closing generators respectively. Referring to the in-plane overlap converter in Fig. 3(b), C_{max} occurs when the overlap between comb electrodes is at a maximum and C_{min} occurs when the overlap is at a minimum. There will be two such energy harvesting cycles within one mechanical oscillation as the comb sets grouped on one side of the central movable mass and the comb sets grouped on the other side of the mass will have their energy conversion cycles 180° out of phase with each other. In Fig. 3(c), for the in-plane gap closing converter, C_{max} occurs when the centre comb finger comes into contact with either the top or bottom comb electrode in one comb set, and C_{min} occurs when the centre comb finger is equidistant from both the top and bottom comb fingers. Similar to the in-plane overlap converter, the in-plane gap closing converter will also have two energy harvesting cycles in one mechanical oscillation as depicted in Fig. 3(c).

Besides, the presence of the electrical isolation in the middle of the movable centre mass in the out-of-plane gap closing structure allows for two energy conversion cycles in one complete mechanical oscillation in Fig. 4(a). Hence, this increases the output energy of the device per vibration cycle. This prospect of having two conversion cycles in one mechanical oscillation is made possible because there are two separate sets of capacitor plates in such a structure, with the first being that of the fixed top cap electrode with the top half of the movable centre mass, and the second set being that of the fixed bottom cap electrode with the bottom half of the movable centre mass. We can use the wafer bonded structure to realize this unique feature. These two energy conversion cycles in one mechanical oscillation can be summarized by the illustration in Fig. 4(b). It is noted that C_{max} occurs when the movable mass is touching either the top or bottom cap electrode, and C_{min} occurs when the movable mass is equidistant from both the top and bottom cap electrode.

For computational purposes, the equations of the maximum and minimum capacitances for each of these individual mechanisms will be presented. For the in-plane overlap generator, the minimum capacitance is assumed to be zero for simplicity if the overlapping area is treated to be zero during C_{min} . Additionally, the maximum capacitance of one comb set can be expressed as

$$C_{\text{max, in-plane overlap}} = 2 \left(\frac{g_i}{\varepsilon_0 A} + \frac{2t}{\varepsilon_{\text{Si}_3\text{N}_4} \varepsilon_0 A_i} \right)^{-1} \quad (10)$$

where ε_0 is the permittivity of free space, $\varepsilon_{\text{Si}_3\text{N}_4}$ is the dielectric constant of silicon nitride, g_i is the distance between adjacent comb electrodes when the electrodes are at their equilibrium positions, t is the thickness of the silicon nitride coating and A_i is the area of overlap between adjacent fingers in one set of comb electrodes. In order to calculate the total effective maximum capacitance involved in one energy cycle, the maximum capacitance for one comb set should be multiplied with the total number of comb sets on one side of the movable mass.

For one comb set in the in-plane gap closing generator, the minimum capacitance takes the same form as the maximum capacitance in the case of the in-plane overlap generator. Hence, the maximum and minimum capacitances can be expressed as

$$C_{\text{max, in-plane gap close}} = \frac{\varepsilon_0 \varepsilon_{\text{Si}_3\text{N}_4} A_i}{2t} + \left(\frac{2g_i}{\varepsilon_0 A_i} + \frac{2t}{\varepsilon_0 \varepsilon_{\text{Si}_3\text{N}_4} A_i} \right)^{-1} \quad (11)$$

$$C_{\text{min, in-plane gap close}} = 2 \left(\frac{g_i}{\varepsilon_0 A} + \frac{2t}{\varepsilon_{\text{Si}_3\text{N}_4} \varepsilon_0 A_i} \right)^{-1} \quad (12)$$

where the parameters of ε_0 , $\varepsilon_{\text{Si}_3\text{N}_4}$, t , g_i and A_i have been defined earlier, but are now in the context of the in-plane gap closing converter. In order to determine the effective maximum and minimum capacitances involved in one energy harvesting cycle, the total number of comb sets on both sides of the movable mass should be multiplied by the maximum and minimum capacitances of one comb set respectively.

Lastly, for the out-of-plane gap closing generator, the maximum and minimum capacitances can be expressed as

$$C_{\text{max, out-of-plane gap close}} = \frac{\varepsilon_0 \varepsilon_{\text{Si}_3\text{N}_4} A_0}{2t} \quad (13)$$

$$C_{\text{min, out-of-plane gap close}} = \left(\frac{2t}{\varepsilon_0 \varepsilon_{\text{Si}_3\text{N}_4} A_0} + \frac{2g_0}{\varepsilon_0 A_0} \right)^{-1} \quad (14)$$

where the parameters of ε_0 , $\varepsilon_{\text{Si}_3\text{N}_4}$, t have been defined earlier, g_0 is the distance between adjacent electrodes when the electrodes are at their equilibrium positions and A_0 is the area of the electrodes.

If the in-plane overlap and in-plane gap closing converters were to be compared, it can be observed that the maximum capacitance of the in-plane overlap converter is very similar to the minimum capacitance of the in-plane gap closing structure. By considering sample comb finger dimensions from the work done by Chiu et al., where $A_0 = 1200 \mu\text{m} \times 200 \mu\text{m}$, $t = 0.05 \mu\text{m}$, $g_0 = 35 \mu\text{m}$, $\varepsilon_{\text{Si}_3\text{N}_4} = 7$, $\varepsilon_0 = 8.854 \times 10^{-12} \text{ Fm}^{-1}$ [14], the maximum capacitance for one set of combs for the in-plane overlap converter will be 0.122 pF, and the minimum capacitance can be treated to be zero. On the other hand, for the same comb finger dimensions, the maximum capacitance will be 0.149 nF and the minimum capacitance will be 0.122 pF for one comb set in the in-plane gap closing generator. By considering Eq. (9), for the same V_{start} and V_{max} , it is observed that the in-plane gap closing generator will have an output that is of the order of 1000 times that of the in-plane overlap generator. Since these two types of generators have similar geometries for similar structural dimensions, it can be concluded from this comparison that the energy output per unit volume for the in-plane overlap generator is very much less than that of the in-plane gap closing mechanism. Hence,

Table 1
The effects of varying the thickness of the load in the in-plane gap closing structure, whilst keeping its mass and the cross-sectional area of the active region constant.

	L_0 (cm)	T_0 (μm)	L_i (cm)	T_i (μm)	W_i (μm)	L_f (μm)	Comb width (μm)	Comb sets on each side of mass
Case 1	1.00	250	1.00	300	7789	1091	15	166
Case 2	1.00	250	1.00	350	6204	1880	17.5	142
Case 3	1.00	250	1.00	400	5017	2472	20	124
Case 4	1.00	250	1.00	450	4093	2931	22.5	110
Case 5	1.00	250	1.00	500	3355	3297	25	99

L_0 : length of mass in the out-of-plane gap closing structure, T_0 : Thickness of mass in the out-of-plane gap closing structure, L_i : Length of mass in the in-plane gap closing structure, T_i : Thickness of mass in the in-plane gap closing structure, W_i : Width of central mass in the in-plane gap closing structure, L_f : Length of comb fingers in the in-plane gap closing structure

the focus of this discussion can just be on comparing the energy output density between the in-plane gap closing and out-of-plane gap closing mechanisms.

4. Modeling consideration and setup

To make a fair comparison, the mass of the movable load in both the in-plane gap closing and out-of-plane gap closing structures is set to be equal. Referring to the resonant frequency of energy harvester, it can be expressed as

$$f = \sqrt{\frac{k}{m}} \quad (15)$$

where f is the resonant frequency of the device, k is the effective spring constant of the connected springs and m is the mass of the movable load. This equation implies that if two devices with identical effective spring constants were to have the same resonant frequency, the mass of the movable loads of these two devices have to be the same. In the design of an energy harvester for a specific application, it is desired for the resonant frequency of the structure to match the vibration frequency of the application for maximum power output. Since the two types of structures are to be designed for the same application, they should have the same resonant frequencies. Hence, it makes sense to set the mass of the movable load to be identical for both the in-plane gap closing and out-of-plane gap closing converters if it is assumed that the effective spring constant for the two cases is designed to be the same. Additionally, if the two devices have the same operating frequencies, we can just make a comparison based on output energy per vibration cycle. Since the output power equals to output energy per cycle multiple with vibration frequency.

One other parameter that will be kept constant between the two devices is the cross-sectional area of the devices' active regions. This is done as typically, in the design of energy harvesters, the applications would require the devices to have a footprint that does not exceed a certain area. Thus, since two devices are being compared for the same application, it makes sense to limit the area that is occupied by the device to a certain value to compare their energy outputs. In particular, for purposes of symmetry, the cross-sectional area of the active region for each device will be set to have its length equal to its width. The constraints that have been set up above will provide a common ground to compare the two mechanisms in terms of the devices' practical realization.

The typically technique for making the silicon based energy harvesters with high aspect ratio is the deep reactive ion etching (DRIE) process technique [23]. The aspect ratio is a critical parameter for comb fingers of the in-plane gap closing structure. The aspect ratio represents etching results of the relationship between the thickness of the centre mass, i.e., the thickness of comb finger, and the etched gap between individual combs fingers. Generally, an aspect ratio of 20:1 is a value that is commonly achievable today, and it implies that the ratio of the thickness of the centre mass to the gap between adjacent comb fingers is 20:1. Thus in this paper, we

deploy aspect ratio of 20:1 as a constraint of defining the comb finger density within a given volume. Therefore, in the case of in-plane gap closing device, we can derive the number of comb fingers when we change the movable centre mass thickness according to a set of equations shown in appendix. The Table 1 shows 5 derived cases of varying the thickness of the mass in the in-plane gap closing structure with assumption of the same movable mass and the same occupied volume of the active region, i.e., the volume encompass the movable mass and comb fingers.

The design of the out-of-plane gap closing structure is relatively straightforward, given that the cross-sectional area of the active region and the mass of the movable electrode are fixed. Thus in Table 1, we fixed the size of 1 cm^2 by $250 \mu\text{m}$ for the movable mass for all cases of the out-of-plane gap closing structure. Therefore, the T_i shown in Table 1 is always larger than T_0 in Table 1.

5. Results and discussion

It is observed from Table 1 that when T_i is increased, the comb width increases while the total number of comb sets decreases. The increase in the comb width can be understood by considering the aspect ratio, since a larger thickness implies that the gap between adjacent combs (and hence the comb width) has to be increased. Additionally, this also implies that the total number of comb sets will decrease as the total length available for these comb fingers remains at a constant value. The abovementioned trends of increasing finger thicknesses and decreasing comb sets have opposing effects on the C_{max} value for the structure, and their effects on C_{max} are resolved and reconciled in the graph in Fig. 5.

In each of the curves in Fig. 5, the effective C_{max} of the in-plane gap closing structure is plotted against T_i , whilst keeping the cross-sectional area of the active region constant at 1 cm^2 and the mass of its movable load at a certain constant value. Additionally, different curves are plotted for loads of different masses. For convenience, the mass of the load describing each of the curves is being defined

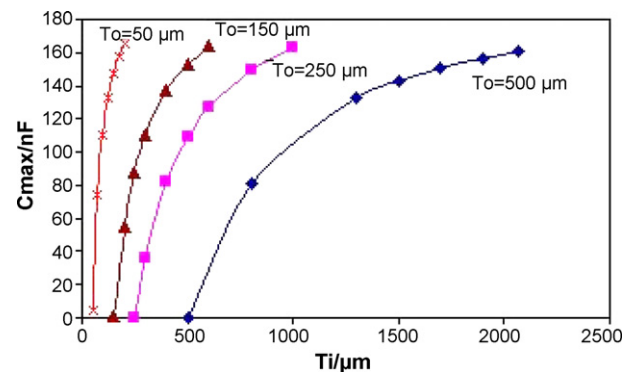


Fig. 5. Graph of the effective C_{max} of the in-plane gap closing structure against the thickness of the mass in the in-plane gap closing structure for different load masses (the different load masses here are defined by the thickness of the equivalent mass in the out-of-plane gap closing structure).

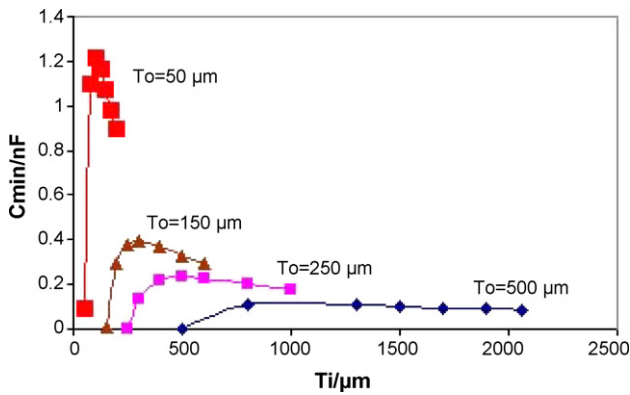


Fig. 6. Graph of the effective C_{min} of the in-plane gap closing structure against the thickness of the mass in the in-plane gap closing structure for different load masses (the different load masses here are defined by the thickness of the equivalent mass in the out-of-plane gap closing structure).

by the thickness of the equivalent load having the same mass in the out-of-plane gap closing structure, T_0 . The masses can be defined as such since the cross-sectional area of the load in the out-of-plane gap closing structure is always assumed to be constant at 1 cm^2 , and its volume (which can be treated as being equivalent to its mass) will thus be directly proportional to its thickness. For example, a $T_0 = 50 \mu m$ label implies that the load in consideration has a volume of 5 mm^3 while a $T_0 = 150 \mu m$ label implies that the load has a volume of 15 mm^3 . During the computation of these parameters, it was observed that within each curve, T_i can only assume values within a specific range as values beyond this range would result in the finger length or the mass width undertaking negative values and being unrealistic. Hence, within each curve, the effective C_{max} for the in-plane gap closing structure is plotted against the entire plausible range of T_i accordingly. Similarly, for different load masses, the effective C_{min} for the in-plane gap closing structure is also plotted against their respective ranges of practical T_i values in Fig. 6.

As shown in Fig. 5, it is observed that the maximum achievable C_{max} for all the four different cases is the same, and they all occur at the maximum realistic thickness value for each case. By comparing the graph in Fig. 5 with that in Fig. 6, it is also noted that the maximum capacitances are of the order of about 100 times that of the minimum capacitances, and this renders the minimum capacitances insignificant in comparison to the maximum capacitances.

In the optimization of the output power, it is necessary to take into account the relationship between the various parameters, C_{max} , C_{min} , C_{par} , V_{start} and V_{max} as well as the circuit constraints. The optimization process can be demonstrated by selecting one set of C_{max} and C_{min} . For illustration purposes, the point at which C_{max} is at its maximum for the case where $T_0 = 250 \mu m$ will be selected. At this particular point, C_{max} is 162.8 nF and C_{min} is 0.174 nF . The 3D graph of V_{max} against C_{par} and V_{start} as well as the 3D graph of energy output against C_{par} and V_{start} are then plotted in Figs. 7 and 8 respectively, in the following ranges $0.1C_{max} \leq C_{par} \leq 2C_{max}$ and $0 \leq V_{start} \leq 5V$.

These ranges are selected by taking into consideration practical circuit constraints. This methodology allows user to select appropriate numbers upon their unique circuits. In present demonstration, we limit the V_{start} to be below 5 V and the V_{max} to below 20 V . With different designs of energy conversion circuits, the appropriate values of V_{start} and V_{max} are different.

In these figures, it is observed that the energy output increases with decreasing C_{par} and increasing V_{start} for any given fixed C_{max} and C_{min} . In the consideration of the V_{start} limitation of 5 V , we can select the optimum value of C_{par} which would give the maximum realizable V_{max} of 20 V . The corresponding energy output would

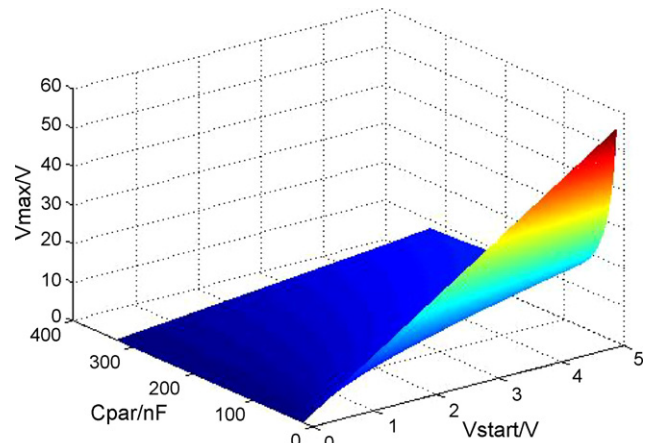


Fig. 7. Graph of V_{max} against V_{start} and C_{par} for a C_{max} of 162.8 nF and a C_{min} of 0.174 nF .

hence be the maximum possible output after having taken into consideration all of the above voltage constraints. In this particular case which has been considered, a C_{par} of 54 nF would give a V_{max} of 20 V and an energy output per cycle of $8.1 \mu J$ for a V_{start} of 5 V . The above steps is repeated for all the other pairs of points in the graphs in Figs. 5 and 6, and the optimum energy output per energy harvesting cycle for the in-plane gap closing structure for different mass values is presented in a graph in Fig. 9. It is observed from

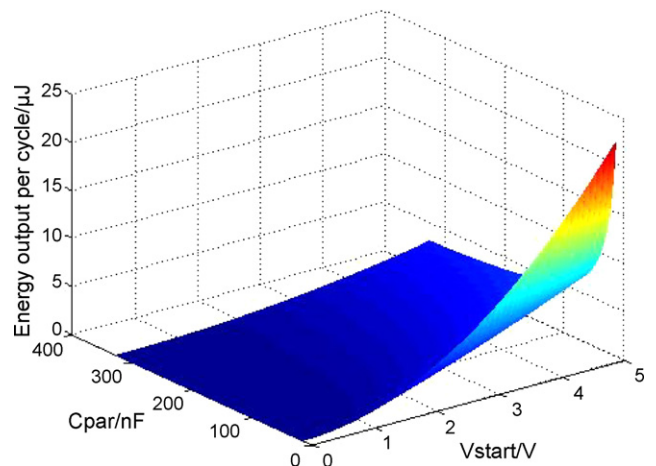


Fig. 8. Graph of energy output per cycle against V_{start} and C_{par} for a C_{max} of 162.8 nF and a C_{min} of 0.174 nF .

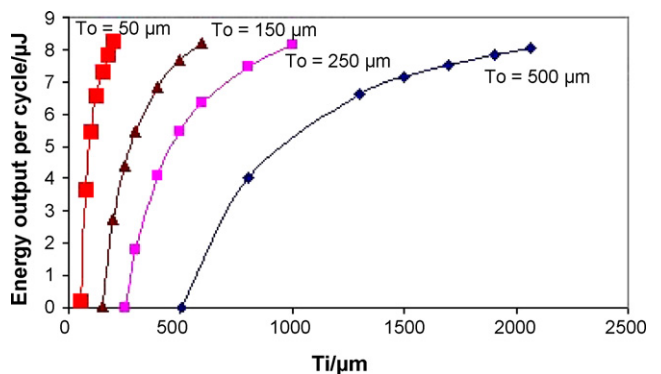


Fig. 9. Graph of energy output per cycle for the in-plane gap closing structure against the thickness of the mass in the in-plane gap closing structure for different load masses (the different load masses here are defined by the thickness of the equivalent mass in the out-of-plane gap closing structure).

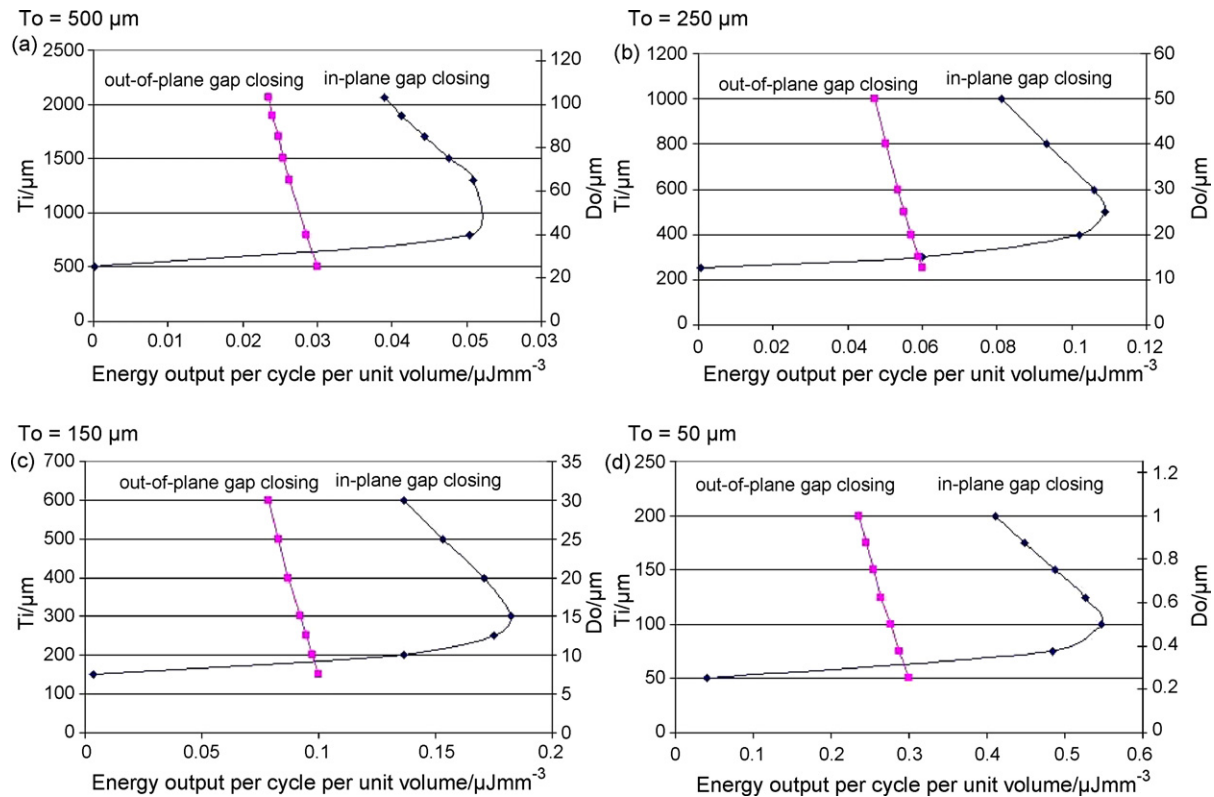


Fig. 10. Graphs of the energy output densities plotted against the thickness of the mass in the in-plane gap closing structure and the maximum mass displacement. The graph when the load has a volume equal to the equivalent load in the out-of-plane structure having (a) $T_0 = 500 \mu\text{m}$, (b) $T_0 = 250 \mu\text{m}$, (c) $T_0 = 150 \mu\text{m}$, and (d) $T_0 = 50 \mu\text{m}$.

Fig. 9 that the maximum energy output per cycle for each of the different loads is the same, and they all occur at the maximum T_i value within each curve.

At the same time, the energy output for the out-of-plane gap closing structure can also be optimized by considering its maximum and minimum capacitances, as well as the same limits of V_{start} and V_{max} . In the calculation of C_{max} and C_{min} for the out-of-plane gap closing structure, reference can be made to Eqs. (13) and (14), respectively. In particular, in the calculation of C_{min} , the g_0 value is treated to be equivalent to the g_i value in the corresponding in-plane gap closing structure. The energy outputs for both the in-plane gap closing and out-of-plane gap closing structures are then normalized against their respective active volumes and the results are plotted in the graphs in Fig. 10.

In Fig. 10, apart from T_i , the normalized energy output is also plotted against the load's maximum displacement in both the in-plane and out-of-plane gap closing structures, D_0 . This displacement

parameter is crucial in determining the active device volume for the out-of-plane gap closing structure as can be seen from Fig. 4(a), and is hence included in the graphs in Fig. 10. From the graphs, it is observed in all four cases that if the thickness of the mass in the in-plane gap closing structure is greater than a certain critical thickness, the energy output density for the in-plane gap closing mechanism is greater than the out-of-plane gap closing mechanism. Additionally, for each of the cases presented, there is an optimum value for the mass thickness in the in-plane structure for which the energy output density of the in-plane gap closing mechanism peaks at a maximum possible value. This is hence evidence that the in-plane gap closing mechanism has the potential to produce a higher amount of energy per unit volume for the same movable load mass and cross-sectional area (of the active region), provided that the thickness of the mass is above a certain critical value. The peak values of the normalized energy outputs are summarized as 0.05 , $0.11 \mu\text{J}/\text{mm}^3$, $0.18 \mu\text{J}/\text{mm}^3$ and $0.55 \mu\text{J}/\text{mm}^3$ for Fig. 10(a)–(d), respectively.

In relation to this, the peak value of the energy output density for the in-plane gap closing and the best value for the out-of-plane gap closing mechanism in various cases of load volumes can be deduced and plotted in Fig. 11. It is observed that the best energy output density for the in-plane gap closing mechanism is always higher than that of the out-of-plane gap closing mechanism for all load volumes between 5 mm^3 and 50 mm^3 . Additionally, the ratio of the best energy output for the in-plane gap closing mechanism to the out-of-plane gap closing mechanism is approximately consistent at 1.8 for load volumes between 5 mm^3 and 50 mm^3 . Mainly due to the contribution of vacuum operation and structural optimization, the normalized energy outputs reported in this paper are also generally higher than that which has been obtained by other groups. The only exception is that the simulated data of energy outputs by Miao et al. has been reported $0.05 \mu\text{J}/\text{mm}^3$ [12]. This value is comparable to that in this paper. It is very likely that the high energy densities

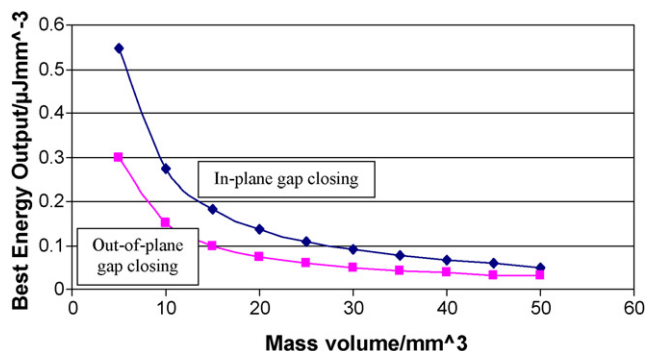


Fig. 11. Curves of the optimum energy output density against to the volume of movable mass.

obtained by Miao et al. [12] can be attributed to their higher V_{\max} values.

6. Conclusion

The focus of this paper differs from previous works in that most of the work hitherto attempts to maximize the power output from their MEMS device by assuming either the in-plane gap closing or the out-of-plane gap closing technique. Instead, this paper presents a systematic method to compare the energy harvesting capabilities between the in-plane gap closing and out-of-plane closing mechanisms. This analytical method thus allows readers to have a basis to select the appropriate MEMS mechanisms in the design of similar devices in order to maximize the power output, when these MEMS energy harvesters are operated in vacuum. For the few cases which have been looked into, it is observed that the in-plane gap closing structure has the potential to produce a higher (approximately 1.6 to 1.8 times) amount of energy per unit volume as compared to the out-of-plane gap closing mechanism, provided the thickness of the mass in the in-plane structure is greater than a critical value. This provides more insight into the energy harvesting capabilities of each technique as the energy output per unit volume is dependent on many parameters, and it is not sufficient to conclude that one technique is generally better than the other. With respect to this, the relations among all the parameters were formulated in this paper. Additionally, the optimum results obtained in this paper have been compared with that reported by other groups, and it has been observed that for the case in which the movable load has a volume of 5 mm^3 (when $T_0 = 50 \text{ }\mu\text{m}$ and $L_i = 1 \text{ cm}$) the energy output density of $0.547 \text{ }\mu\text{J mm}^{-3}$ is approximately 6.5 times that of the highest reported data from other groups.

Acknowledgements

Authors would like to thank A*STAR HOME 2015 National Research Programme (SERC grant number: 0621150043) for the funding of this project and in-kind contribution from Institute of Microelectronics, A*STAR.

Appendix A.

We consider two onstraints in our mathematic model in which the movable loads are set to have equal masses, and the aspect ratio is set as 20:1. In addition, to simplify the mathematical model, there is an assumption that the numerical value of the comb fingers' width is equivalent to the gap between adjacent comb fingers. Thus the following equation can be derived

$$L_0^2 T_0 = W_i L_i T_i + \frac{20L_i - T_i}{40} L_f T_i \quad (16)$$

where L_0 and T_0 are the length and the thickness of the movable mass respectively in the out-of-plane gap closing structure, and L_i , W_i , T_i and L_f are the length of the active region's cross-sectional area, the width and the thickness of the centre movable mass and the length of the comb fingers respectively in the in-plane gap closing structure.

For the constraint in which the cross-sectional area of the active regions have the same dimensions, and referring to Figs. 3 and 4(a), there are the equations

$$L_i = L_0 \quad (17)$$

$$2L_f + W_i + 2\frac{T_i}{20} = L_i \quad (18)$$

By setting the independent parameters to be L_0 , T_0 , L_i , and T_i , and the dependent parameters to be W_i and L_f , the dependent variables

can be written as a function of the independent variables as such

$$L_f = \frac{40L_i^2 T_i - 40L_0^2 T_0 - 4L_i T_i^2}{T_i^2 + 60L_i T_i} \quad (19)$$

$$W_i = L_i - \frac{80L_i^2 T_i - 80L_0^2 T_0 - 8L_i T_i^2}{T_i^2 + 60L_i T_i} - \frac{T_i}{10} \quad (20)$$

For the purposes of defining the active device volume which will be considered in the normalization of energy later, an additional constraint is set up to equate the displacement of the mass in the out-of-plane gap closing mechanism to be equal to that of the mass in the in-plane gap closing mechanism. This implies that the amplitude of vibration of the movable masses in each of the two mechanisms is set to be the same. With reference to Figs. 3 and 4(a), as well as the consideration of the aspect ratio of 20:1, the following equality then can be obtained

$$D_0 = \frac{T_i}{20} \quad (21)$$

where D_0 is the gap between two adjacent electrode plates in the out-of-plane gap closing structure.

References

- [1] S.P. Beeby, M.J. Tudor, N.M. White, Energy harvesting vibration sources for microsystems applications., *Measurement Sci. Technol.* 17 (2006) 175–195.
- [2] S. Roundy, P.K. Wright, J. Rabaey, A study of low level vibrations as a power source for wireless sensor nodes, *Comput. Commun.* 26 (2003) 1131–1144.
- [3] S. Roundy, On the effectiveness of vibration-based energy harvesting, *J. Intell. Mater. Syst. Struct.* 16 (2005) 809–823.
- [4] H.B. Fang, J.Q. Liu, Z.Y. Xu, L. Dong, L. Wang, D. Chen, B.C. Cai, Y. Liu, Fabrication and performance of mems-based piezoelectric power generator for vibration energy harvesting, *Microelectron. J.* 37 (2006) 1280–1284.
- [5] M. Ferrari, V. Ferrari, M. Guizzetti, D. Marioli, A. Taroni, Piezoelectric multifrequency energy converter for power harvesting in autonomous Microsystems, *Sens. Actuators A* 142 (2008) 329–335.
- [6] E. Lefevre, A. Badel, C. Richard, L. Petit, D. Guyomar, A comparison between several vibration-powered piezoelectric generators for standalone systems, *Sens. Actuators A* 126 (2006) 405–416.
- [7] C.B. Williams, R.B. Yates, Analysis of a micro-electric generator for Microsystems, *Sens. Actuators A* 52 (1996) 8–11.
- [8] S. Shearwood, R.B. Yates, Development of an electromagnetic micro-generator, *Electron. Lett.* 33 (1997) 1883–1884.
- [9] D.P. Arnold, Review of microscale magnetic power generation, *IEEE Trans. Magn.* 43 (2007) 3940–3951.
- [10] N.S. Hudak, G.G. Amatuucci, Small-scale energy harvesting through thermoelectric, vibration, and RF power conversion, *J. Appl. Phys.* 103 (2008) 101301.
- [11] S. Meninger, J.O. Mur-Miranda, R. Amirtharajah, A.P. Chandrakasan, J.H. Lang, Vibration-to-electric energy conversion, *IEEE Trans. Very Large Scale Integr. (VLSI) Syst.* 9 (2001) 64–76.
- [12] P. Miao, P.D. Mitcheson, A.S. Holmes, E.M. Yeatman, T.C. Green, B.H. Stark, MemS inertial power generators for biomedical applications, *Microsyst. Technol.* 12 (2006) 1079–1083.
- [13] I. Kuehne, A. Frey, D. Marinkovic, G. Eckstein, H. Seidel, Power MEMS-A capacitive vibration-to-electricity energy converter with built-in voltage, *Sens. Actuators* 142 (2008) 263–269.
- [14] Y. Chiu, C.T. Kuo, Y.S. Chu, MemS design and fabrication of an electrostatic vibration-to-electricity energy converter, *Microsyst. Technol.* 13 (2007) 1663–1669.
- [15] Y. Chiu, V.F.G. Tseng, A capacitive vibration-to-electricity energy converter with integrated mechanical switches, *J. Micromech. Microeng.* 18 (2008) 104004.
- [16] P.D. Mitcheson, E.M. Yeatman, G.K. Rao, A.S. Holmes, T.C. Green, Energy harvesting from human and machine motion for wireless electronic devices, *Proc. of the IEEE* 96 (2008) 1457–1486.
- [17] M. Esashi, Wafer level packaging of MEMS, *J. Micromech. Microeng.* 18 (2008) 073001.
- [18] K. Minami, T. Moriuchi, M. Esashi, Cavity pressure control for critical dumping of packaged micro mechanical devices, in: *Dig. Tech. Papers, Transducers'95* (Stockholm, Sweden), 1995, pp. 240–243.
- [19] R. Gooch, T. Schimert, Low-cost wafer-level vacuum packaging for MEMS, *MRS Bull.* 28 (2003) 55–59.
- [20] C. Lee, A. Yu, L. Yan, H. Wang, J.H. Han, Q.X. Zhang, J.H. Lau, Characterization of intermetallic compound of In/Ag solder based low temperature fluxless wafer bonding for MEMS packaging, *Sens. Actuators A*, in press, doi:10.1016/j.sna.2008.10.011.
- [21] <http://www.sitime.com/>.
- [22] P. Monajemi, P.J. Joseph, P.A. Kohl, F. Ayazi, Wafer-level MEMS packaging via thermally released metal-organic membranes, *J. Micromech. Microeng.* 16 (2006) 742–750.

- [23] S.A. McAuley, H. Ashraf, L. Atabo, A. Chambers, S. Hall, J. Hopkins, G. Nicholls, Silicon micromachining using a high-density plasma source, *J. Phys. D: Appl. Phys.* 34 (2001) 2769–2774.

Biographies

Chengkuo Lee received a MS degree in materials science and engineering from National Tsing Hua University, Hsinchu, Taiwan, in 1991. He also received a MS degree in industrial and system engineering from Rutgers University, New Brunswick, NJ, USA in 1993. He received the PhD degree in precision engineering from the University of Tokyo, Tokyo, Japan, in January 1996. He worked in Mechanical Engineering Laboratory, AIST, MITI of Japan as a research fellow of Japan Science and Technology Agency (JST) in 1996. Since September 1997, he has joined the Metrodyne Microsystem Corporation, Hsinchu, Taiwan, and established the MEMS device division and micromachining fabrication. He was the manager of MEMS device division between 1997 and 2000. He had been the adjunct assistant professor in Electro-physics Department at National Chiao Tung University in 1998, and the adjunct assistant professor in Institute of Precision Engineering at National Chung Hsing University from 2001 to 2005. He co-founded Asia Pacific Microsystems, Inc. (APM) Hsinchu, Taiwan, R.O.C., in August 2001, and he became the Vice President (VP) of R&D, then the VP of optical communication business unit. Currently, he is an Assistant Professor at the Department of Electrical and Computer Engineering at the National University of Singapore and a Senior Member of Technical Staff at the Institute of Microelectronics (IME), Agency for Science, Technology and Research (A*STAR), Singapore. He has contributed more than 170 international conference papers and international journal articles in MEMS and nanotechnology fields. He is the member of IEEE, MRS, and IEE Japan. He received the IUMRS graduate student award in 1994.

Ye Mei Lim received her BSc degree from Department of Electrical and Computer Eng at National University of Singapore in 2008.

Bin Yang received the BS degree in Materials Science from Anhui University of Technology and Science, China. He received his MS degree in Materials Science from Jilin University in 2003 and PhD degree in Electronic Science and Technology from Shanghai Jiao Tong University in 2006, China. From August 2006 to October 2007, he was employed as a Research Fellow at the Department of Mechanical Engineering, National University of Singapore. He is currently a Senior Search Engineer at the Institute of Microelectronics (IME). His research interests include energy harvesters, optical MEMS, piezoelectric actuators and sensors.

Rama Krishna Kotlanka has obtained bachelor of mechanical engineering (Hons) from University of Madras, India in 2001; Master of Science in Computer Integrated Manufacturing and PhD from Nanyang Technological University, Singapore in 2003

and 2006 respectively. Since then, he is with A*Star Institute of Microelectronics, Singapore working on micro-electro-mechanical Systems for biomedical applications. His research interests include, sensors for robotic surgery, mechanobiology, biomechanics of skeletal fracture fixation and spine, and smart implants.

Chun-Huat Heng received the BEng and MEng degrees from the National University of Singapore in 1996 and 1999, respectively, and the PhD degree from the University of Illinois at Urbana-Champaign in 2003. From 2001 to 2004, he was with Wireless Interface Technologies, which was later acquired by Chrontel. Since 2004, he has been with the National University of Singapore. He has been working on CMOS integrated circuits involving the synthesizer, transceiver, and receiver architectures for communications systems.

Johnny Han He received his PhD in MEMS in Cambridge University Engineering Department, UK. He also holds MSc in Advanced Material in Micro-/Nano- System from NUS and MIT of Singapore-MIT Alliance, and BEng in Electrical Engineering from Shanghai Jiao Tong University, P.R. China. He is currently working as Senior Research Engineer in Institute of Microelectronics, Singapore. His research interest is in micro-fabrication, characterization, design and simulation of advanced microsystem. He is also a Member of Institute of Electrical Engineer (MIEE), Member of Institute of Electronics and Electrical Engineer (MIEEE) and Associate Member of Institute of Physics (AMInstP).

Min Tang received her PhD degree in MEMS and Microelectronics from Nanyang Technological University in 2007. She received her MSc degree in Microelectronics and Solid-state Electronics in 2001 and BEng degree in Applied Chemistry in 1998, both from Shanghai Jiao Tong University. Currently she is the Senior Research Engineer at Institute of Microelectronics, Singapore. Her research interests include MEMS device design, simulation and fabrication.

Jin Xie received his bachelor degree in automotive engineering from Tsinghua University, China, in 2000 and master degree in mechanical engineering from Zhejiang University, China, in 2003, and obtained PhD from Nanyang Technological University, Singapore, in 2007. He is currently working in Institute of Microelectronics, A*STAR, Singapore. His research interests involve design of micro sensors and actuators, micro fabrication, energy harvester and dynamic testing.

Hanhua Feng received her Bachelor's degree in 1985, Master of Engineering in 1988, and PhD in Engineering in 1992, all from Huazhong University of Science and Technology (HUST), Wuhan, P.R. China. She is a manager leading the MEMS task in Institute of Microelectronics (IME), Agency for Science, Research and Technology (A*STAR), Singapore. Her current fields of interest are micro-fabrication technologies for MEMS and NEMS.